Versatile Metal Nanowiring Platform for Large-Scale Nano- and Opto-Electronic Devices

*Yeongjun Lee, Sung-Yong Min, Tae-Sik Kim, Su-Hun Jeong, Ju Yeon Won, Hobeom Kim, Wentao Xu, Jae Kyeong Jeong, and Tae-Woo Lee**

Highly conductive 1D metal nanowiring is a core technology for the manufacture of highly integrated microcircuits as well as wire bonding interconnection of 3D stacked electronic devices. For that purpose, control of nanoscale conductive metal wires (representatively Ag nanowires (AgNWs)) with desired position and orientation is a critical issue. Previously reported AgNWs-fabrication techniques such as chemically synthesized (length < 50 µm) Type I AgNWs (**Figure 1**a) and randomly oriented nonwoven electrospun Type II AgNWs (Figure 1b) do not control their orientation and position individually, so those AgNWs cannot be used as individual 1D nanoscale electrodes (nanoelectrodes) array of circuits, only can be used in randomly dispersed 2D sheet-type transparent electrodes due to short length and individual uncontrollability requiring additional patterning processes.[1–10] Even though 2D sheet-type electrodes composed of randomly oriented 1D NWs have been emerged as a strong alternative to replace conventional indium tin oxide (ITO) electrodes based on their low sheet resistance $10 \le R_S \le 50\ \Omega\ \text{sq}^{-1}$, high optical transmittance $T > 80\%$, and facile solution processes, they have limitations such as low uniformity (Figure 1c,d), excessive surface roughness, and reduced transparency caused by optical haze (diffusive transmittance/total transmittance) due to light scattering.[1–10] Moreover, high-volume production with short AgNW-based devices is impeded by drawbacks such as high price of AgNWs, requirement of additional lithographic patterning processes,[11] and thermal instability in air over 200 °C[12] which is occasionally required for post-annealing process of materials on the electrodes, e.g., formation of inorganic metal oxide semiconducting films. Existing NW alignment techniques do not position AgNWs in a precisely controlled manner in large area for use as 1D nanoelectrode arrays.[13] Therefore, development of individually position-addressable and pattern-customizable metal nanowiring technology is highly desired.

Here, we report a novel Ag nanowiring platform of large-scale-aligned AgNWs (Type III) with efficient material utilization, high throughput, low processing cost, and simple direct printing procedures. The Ag nanowiring on the desired position processed in an individually controlled manner (Figure 1e) allows development of the AgNWs as both 1D nanoelectrodes of electronic circuits and 2D large-scale transparent electrodes of optoelectronic applications, so it overcomes many limitations of conventional Type I and II AgNWs. Our printed AgNWs have an average diameter of ≈695 nm and are therefore invisible to the naked eye. Also, low resistivity ($\rho = 5.7\ \mu\Omega$ cm) of AgNWs is comparable to that of bulk Ag ($\rho = 1.6\ \mu\Omega$ cm). Based on these properties, highly aligned AgNW array with grid pitch size of 100 µm showed low sheet resistance ($R_S \approx 26.9\ \Omega\ \text{sq}^{-1}$), high transmittance ($T \approx 94.7\%$), low optical haze (≤1%) at wavelength (λ) of 550 nm, high thermal stability in air (up to 350 °C), and mechanical flexibility.

The reliable electronic wiring of large-scale AgNWs in varied forms of 1D and 2D nanoelectrodes leads to the considerable achievement of a novel electronic application. With versatile Ag nanowiring, we successfully achieved a large-scale all-nanowire field-effect transistor (all-NW FET) array with a high field-effect hole mobility ($\mu_h = 2.08$ cm^2 V^{-1} s^{-1}); the all-NW FET consists of two strands of aligned AgNW as source/drain (S/D) 1D nanoelectrodes and highly aligned poly(3-hexylthiophene-2,5-diyl) (P3HT) NWs as an active channel. The hole mobility achieved using a non-ionic gate dielectric is very high compared to the previous literature commonly reported values of $0.01 \le \mu_h \le 0.3$ cm^2 V^{-1} s^{-1} in P3HT thin films and wires based devices.[14] We also fabricated thin film FETs that use AgNW S/D 1D nanoelectrodes and indium zinc oxide (IZO, *n*-type) or pentacene (*p*-type) layer as active channels; they exhibited reasonable field-effect carrier mobilities ($\mu_e = 7.25$ cm^2 V^{-1} s^{-1} for IZO, $\mu_h = 0.27$ cm^2 V^{-1} s^{-1} for pentacene). Moreover, 2D sheet-type AgNW transparent electrodes were utilized for the demonstration of organic light-emitting diodes (OLEDs), transparent heaters, and touch screen panels (TSPs) which proved the wide applicability of AgNW nanoelectrodes.

The novel Ag nanowiring platform of Type III AgNWs was produced by polymer-assisted continuous and aligned metal-NW printing (PCAMP) using an electric-field-induced NW printer.[14,15] PCAMP uses a strong electric field to eject a mixture solution of high molecular weight polyvinyl pyrrolidone (PVP, $M_W = 1\,300\,000$ g mol^{-1}) and metal precursors from the nozzle of a syringe; high molecular weight polymer enables continuous printing of long nanowires without breaks. Solvents are evaporated during jetting and solidified polymer/metal precursor composite NWs are collected on a substrate that is mounted on a grounded collector. A computer-controlled

---

Y. Lee, Dr. S.-Y. Min, Dr. T.-S. Kim, S.-H. Jeong, H. Kim, Dr. W. Xu, Prof. T.-W. Lee
Department of Materials Science and Engineering
Pohang University of Science and Technology (POSTECH)
Pohang, Gyeongbuk 37673, Republic of Korea
E-mail: twlee@postech.ac.kr, taewlees@gmail.com

J. Y. Won
Department of Materials Science and Engineering
Inha University
Incheon 22212, Republic of Korea

Prof. J. K. Jeong
Department of Electronic Engineering
Hanyang University
Seoul 04736, Republic of Korea

DOI: 10.1002/adma.201602855

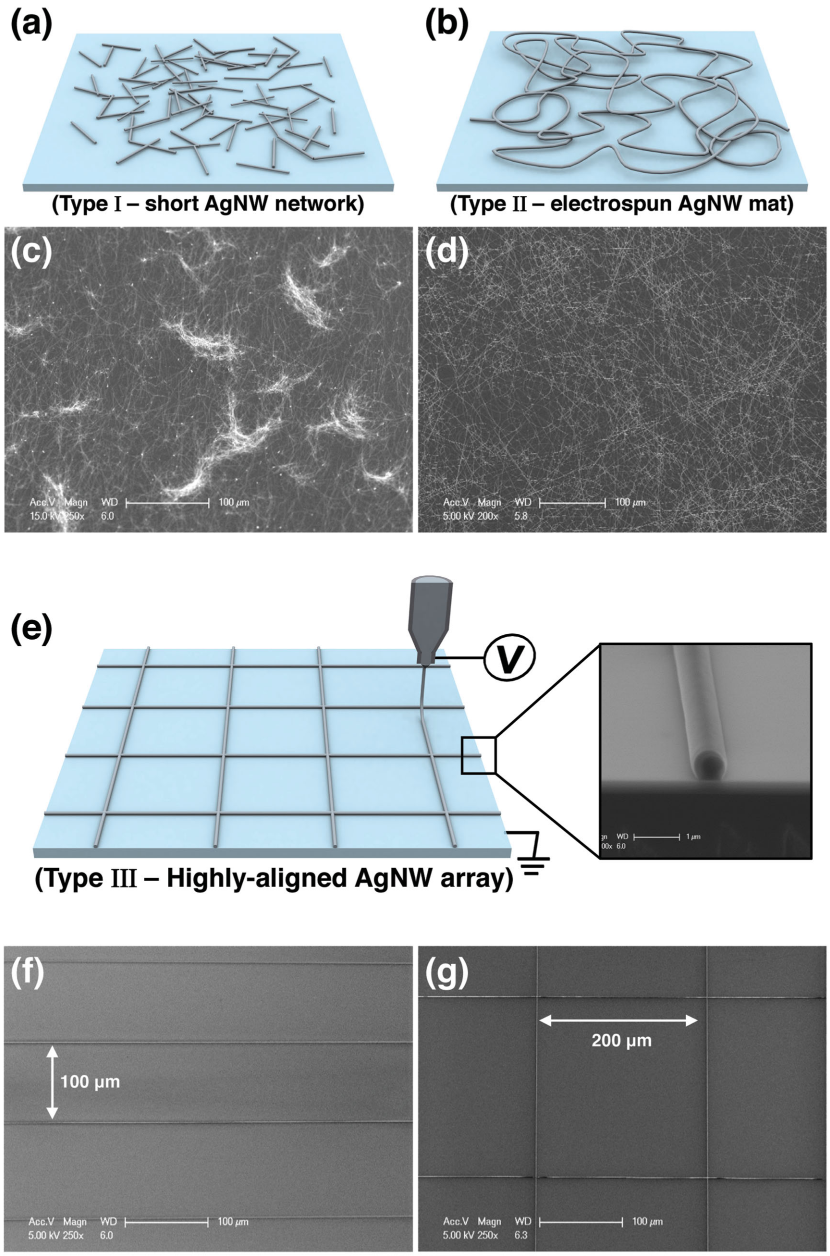

Figure 1. A novel Ag nanowiring platform. Schematic illustration of a) a randomly dispersed short AgNW network (Type I) and b) a randomly oriented electrospun AgNW mat (Type II). SEM images of c) a Type I AgNW network and d) a Type II AgNW mat, which showed low uniformity of AgNWs. e) Schematic illustration of a novel highly aligned and pattern-customizable AgNW array (Type III) (right: SEM image of a composite NW). SEM images of f) stripe-patterned and g) grid-patterned AgNW arrays (scale bar: 100 μm).

robotic stage is moved appropriately to achieve the desired orientation and position of the NWs (Figure S1, Supporting Information); this nanowiring yields a highly aligned and long continuous polymer/precursor composite NW array. After one calcination step in ambient air (350 °C; 20 min), the polymer is decomposed and the metal precursors are converted to metal NWs. Because Ag has relatively lower melting temperature (≈961 °C) than other metals (Cu ≈1083 °C, Au ≈1063 °C, Cr ≈1615 °C, and Ni ≈1453 °C) as well as high resistance to oxidation in air, the printed composite NWs are transformed to metallic AgNWs at relatively low calcination temperature (350 °C) without reduction process under the H_2 gas condition, which is different from previously reported randomly coiled electrospun metal nanofibers.[6,7] The metal precursors are composed of silver trifluoroacetate (STA) and copper trifluoroacetate (CTA) (4:1, w:w). It is because the Ag component agglomerates easily at high temperature, AgNWs from PVP/STA separated after calcination (Figure S2, Supporting Information).[9] To prevent disconnection of NW, a supporting frame which maintains a continuous structure during thermal annealing is necessary. A metal oxide with high melting temperature was expected to fulfill this function effectively, so we mixed CTA with STA to build a CuO frame structure. AgNWs from PVP/STA/CTA had an average diameter of 695 ± 126 nm (measured with more than 80 wires, Figure S3a, Supporting Information) and a cylindrical structure with high aspect ratio (length-to-width ratio, $>10^5$ with 10 cm long NW) that can be freely controlled by adjusting the wiring length from a few millimeter to tens of centimeters in our current setup. The deviation of diameter can be attributed to several experimental parameters and environments including inevitable fluctuations in solution feeding flow, electric field during stage moving, temperature, humidity, and air flow which directly influence the evaporation of solvent for deciding the diameter of nanowires (Figure S3b–g, Supporting Information). By controlling the movement of the grounded collector along the *x*- and *y*-axes, we fabricated pattern-customized Ag nanoelectrode arrays in the forms of highly aligned parallel stripe, perpendicular grid, and curved waves (Figure 1f,g and Figure S4, Supporting Information).

The single AgNW had extremely low electrical resistivity $\rho = 5.7$ μΩ cm (average resistivity = 6.7 ± 0.9 μΩ cm), which is of the same order of magnitude as bulk Ag (1.6 μΩ cm) (**Figure 2**a) and comparable with previously reported printed Ag electrodes;[16] the resistivity was not affected by a length of the NW (Figure S5, Supporting Information). The pitch size of Ag nanowiring can be simply controlled by adjusting the printing parameters, so we fabricated parallel stripe and perpendicular grid patterns with pitch sizes of 100, 200, 400, and 800 μm. Based on nanoscale width and low resistivity of AgNW, transparent grid electrode (100 μm pitch) had $R_S = 26.9$ Ω sq^{-1} and low optical haze (<1%) at high $T = 94.7\%$ (at $\lambda = 550$ nm) (Figure 2b–d). These characteristics are comparable with those of conventional ITO[17] and better than those of alternative

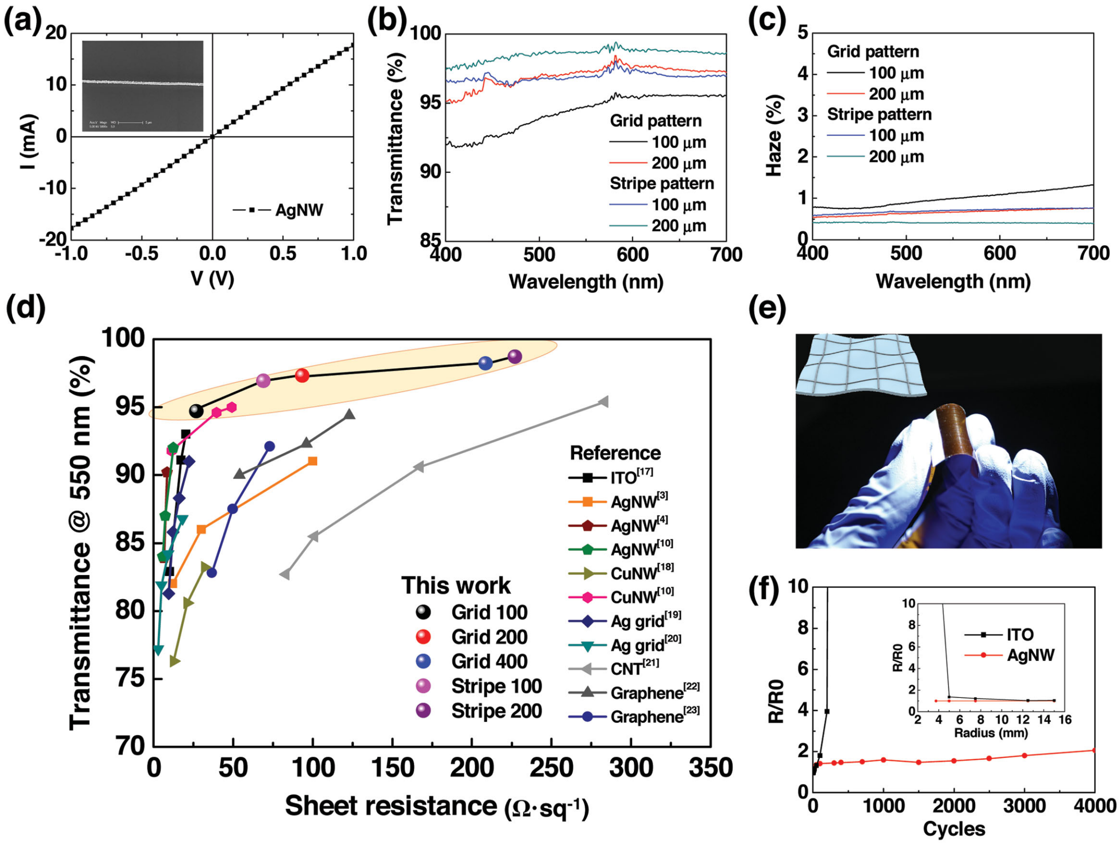

Figure 2. Characteristics of AgNWs. a) Current–voltage (*I*–*V*) curve of AgNW. The resistivity of AgNW was 5.7 μΩ cm (inset: SEM image of a single AgNW). b) Optical transmittance and c) haze characteristics of AgNW arrays with different patterns and pitch size in the visible range. d) Transmittance (at 550 nm) versus sheet resistance for AgNW arrays with ITO[17] and various alternative transparent electrodes fabricated without vacuum evaporation processes such as conventional AgNWs,[3,4,10] CuNWs,[10,18] printed Ag grids,[19,20] carbon nanotubes,[21] and graphene.[22,23] e) Digital image of AgNW array on flexible PI film. f) Bending stability test of AgNW/PI and ITO/PET against bending cycles with bending radius of 7.5 mm (inset: R_S vs bending radius of AgNW array and ITO).

transparent electrodes such as metallic NWs,[3,4,10,18] printed metal grid,[19,20] carbon nanotube (CNT),[21] and graphene (Figure 2d and Tables S1 and S2, Supporting Information).[22,23] These results demonstrate the strong competitiveness of AgNW array as an alternative transparent electrode.

The mechanical bending stability of AgNW array electrode printed on polyimide (PI) substrate was superior to that of an ITO electrode on polyethylene terephthalate (PET) substrate (Figure 2e,f). With a bending radius of 7.5 mm, R_S of Ag nanoelectrode array was not much changed after 4000 bending cycles, whereas the R_S of the ITO electrode on PET substrate increased drastically after ten cycles (Figure 2f). With a bending radius less than 3.75 mm, AgNW electrodes were more durable than the conventional ITO/PET electrode. AgNWs also had an excellent air stability, with R_S was unchanged after aging in ambient air (RH ≈ 50%) for one month (Figure S6, Supporting Information).

The novel AgNW array (Type III) was superior to the previous tangled AgNW networks (Type I and II) and printed metal grid transparent electrodes in several aspects (Table S2, Supporting Information). First, well-aligned AgNW arrays overcame the optical haze that is an intrinsic problem due to huge light scattering in high density percolation of conventional randomly dispersed AgNW networks. The Type III AgNW arrays with various pitch sizes showed low average optical haze ≤1% (Figure 2c) due to their high transmittance and low light scattering, because long and continuous AgNW arrays did not need a high-density percolating network. Second, our AgNW arrays can be used as 2D sheet-type electrodes for optoelectronic devices as well as 1D line-type nanoelectrodes for large-scale highly integrated electronic circuits because AgNWs can be positioned individually at the desired location and orientation. Third, the pattern-designable nanosized metal wire grid is invisible to the naked eye, so it avoids the reduction in visibility and the moiré fringe effect which are caused by the conventional thick metal grid patterns. Fourth, the fabrication procedure of solution-based direct printing is simple, fast (≈33.3 cm s^{-1}), scalable, and cost-effective due to a very low material consumption compared with currently available electrode fabrication methods such as vacuum deposition, lithography,[24] drop-on-demand printing,[25] contact printing,[26] and other 1D or 2D nanostructure preparation techniques.[1,27]

We developed electronic applications using Ag nanowiring platform. We proved the feasibility of a single AgNW as a 1D nanoelectrode for large-scale electronic device array

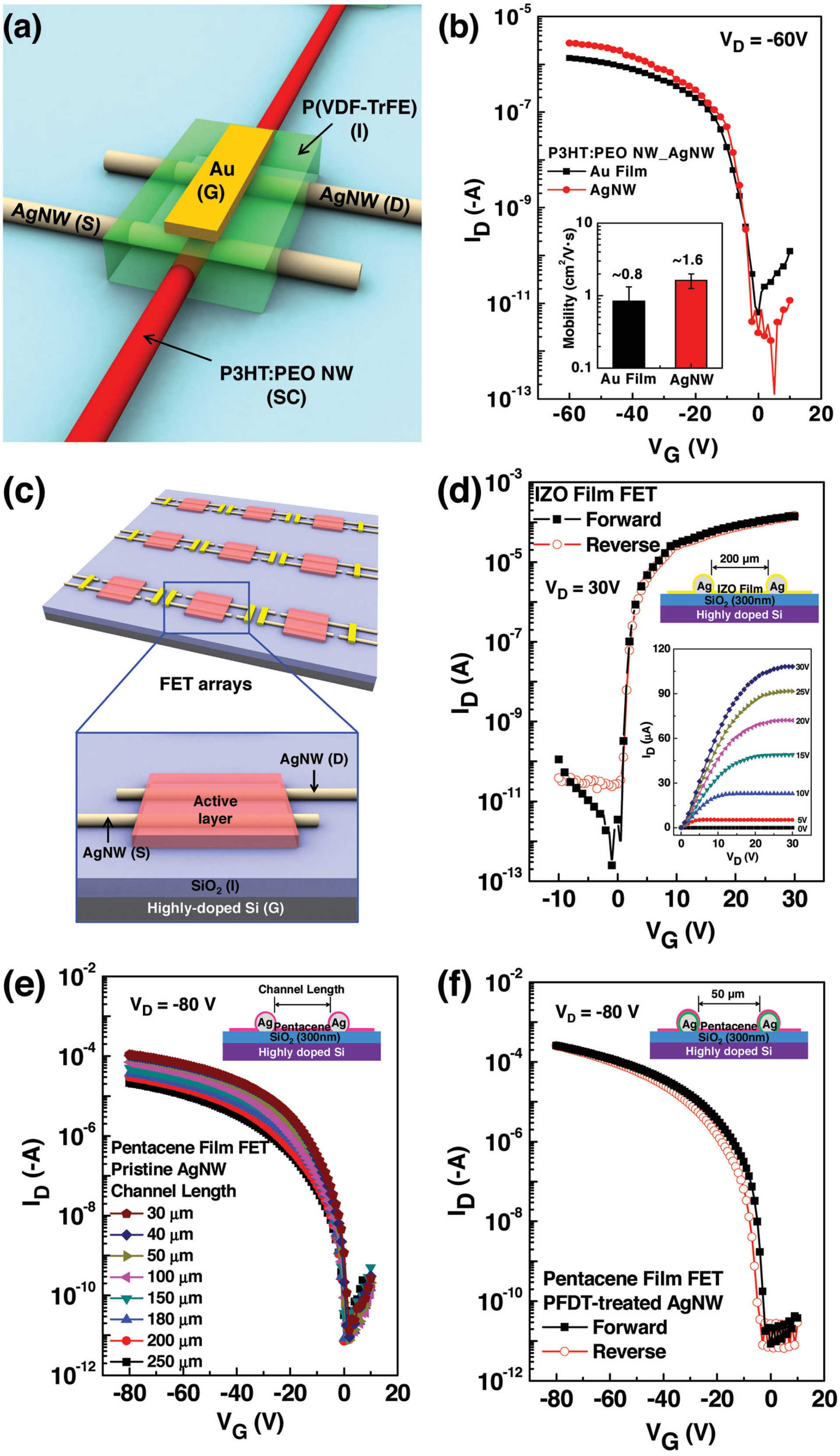

Figure 3. FETs with AgNW 1D S/D nanoelectrodes. a) Schematic illustration of specific device structure of all-NW FETs composed of P3HT semiconducting NW as an active channel printed on the AgNW S/D nanoelectrodes and P(VDF-TrFE) gate insulator.

by fabrication of an all-NW-based transistor array with semiconducting P3HT NWs as an active channel and conducting AgNWs as S/D electrodes (**Figure 3**a). Before P3HT NWs were printed on the two strings of AgNWs, Au contact pads (50 nm) for electrical contacts were deposited, and the S/D nanoelectrodes were defined by cutting each end of continuous AgNWs. A poly(vinylidene fluoride-trifluoroethylene) (P(VDF-TrFE)) dielectric layer (500 nm) was spin-coated on the NWs and Au gate electrodes (50 nm) were deposited on top of the assembly (Figure S7, Supporting Information). Due to the high dielectric constant of P(VDF-TrFE) and top-gate structure, the all-NW transistor had high μ_h up to 2.08 cm^2 V^{-1} s^{-1} (average = 1.63 ± 0.38 cm^2 V^{-1} s^{-1}) without hysteresis (Figure 3b). μ_h was higher in the FET with AgNW electrodes than in the FET with Au film S/D electrodes because AgNWs have a higher work function (WF) (≈5.1 eV) than does Au film in air (≈4.7 eV),[28,29] as verified by Kelvin probe measurement (Figure S8, Supporting Information). The WF of AgNWs is also closely matched with that of the highest occupied molecular orbital of P3HT (≈5.2 eV).[30]

Printed AgNWs have higher WF than Ag films (≈4.3 eV)[28,31] and Au films in air because the NWs include CuO which has a deep valence band edge (≈5.42 eV).[32] X-ray photoelectron spectroscopy (XPS) of both the printed AgNW and the vacuum-deposited Ag film showed binding energies of Ag 3d$_{5/2}$ at 368.2 eV and Ag 3d$_{3/2}$ at 374.2 eV, which correspond to pure metallic Ag (Figure S9a,b, Supporting Information).[33] However, in the O 1s spectrum, AgNW had three clear peaks at binding energies of 529.7, 531.4, and 532.9 eV, which are originated from the O in CuO, in Cu(OH)$_2$, and in a small amount of adsorbed H$_2$O molecules on the surface of AgNW, respectively,[34] whereas the Ag film had a small peak at 530.4 eV that is attributed to O adsorbed to the electrophilic state of Ag (Figure S9c, Supporting Information).[35] The Cu 2p spectra of AgNW also clearly showed the existence of CuO in AgNW with the Cu 2p$_{3/2}$ (933.7 eV) and Cu 2p$_{1/2}$ (953.5 eV) peaks from CuO, and two CuO/Cu(OH)$_2$ satellite peaks (Figure S9d, Supporting Information).[34] These results suggest that CuO both provides a structure supporting frame, and tunes the WF of AgNW. Consequently, the all-NW FETs with AgNW electrodes had better electrical characteristics than the devices with Au film electrodes. This work is the first demonstration of a large-scale all-NW transistor array fabricated by direct printing.

We also demonstrated bottom-contact, bottom-gate (BCBG) thin film FETs with two kinds of semiconducting thin films that were deposited on the AgNWs (Figure 3c): one was IZO (35 nm) which is an *n*-type inorganic semiconductor; the other was pentacene (50 nm) which is a *p*-type organic semiconductor. AgNWs were thermally stable when the IZO thin film on AgNWs was post-annealed at high temperature in air (250 °C, 1 h); this means that printed AgNWs are more thermally stable than conventional AgNWs which disconnect during annealing at 200 °C in air.[12] IZO FETs with the printed AgNW electrodes showed typical n-type transfer and output behavior with field-effect electron mobility μ_e up to 7.25 cm^2 V^{-1} s^{-1} (average = 5.49 ± 1.47 cm^2 V^{-1} s^{-1}) and high on/off current ratio of 5.93 × 10^8 (Figure 3d). The μ_e is lower than that of conventional IZO thin film transistors (>20 cm^2 V^{-1} s^{-1})[36] because the high WF of AgNW (≈5.1 eV) did not match with the conduction band edge of the n-type IZO semiconductor (3.45 eV), which resulted in a non-Ohmic contact in the output characteristics curve (Figure 3d, inset).[37] However, it is still high enough to use as an alternative for a-Si TFT ($\mu \approx 1$ cm^2 V^{-1} s^{-1}) to operate a commercial display.

The channel length L of FETs was easily controlled by printing AgNWs at different spacings. The minimum channel length we can achieve is related to the minimum step movement resolution of the robotic stage motor in our NW printing system (PCAMP), which is currently 3 µm. However, there were several constraints which hinder the reliable formation of short wire spacing (<30 µm): (i) vibration of a high-speed robotic stage, (ii) electrostatic repulsion between charged NWs, and (iii) jet perturbation due to air flow and external electric field. We fabricated pentacene FETs with various channel lengths $30 \le L \le 250$ µm using pristine AgNWs or surface-modified AgNWs by a self-assembled monolayer with fluorine moiety (1H,1H,2H,2H-perfluorodecanethiol, PFDT) which increases the WF of the electrode by surface dipole moments (Figure 3e,f and Figure S10, Supporting Information).[31] PFDT treatment of AgNW electrodes decreased the energy barrier and contact resistance R_C (from 0.94 to 0.079 MΩ cm) at the interface between the pentacene and AgNWs (Figure S11, Supporting Information) and therefore increased μ_h in FETs to 0.27 cm^2 V^{-1} s^{-1} (L = 100 µm), which is much higher than in devices with pristine AgNWs (μ_h = 0.1 cm^2 V^{-1} s^{-1}) (Table S3, Supporting Information). The pentacene FET with PFDT-treated AgNW electrodes did not show significant degradation of maximum drain current and mobility after repeated tests (Figure S12, Supporting Information). This successful fabrication of conventional inorganic and organic thin film transistors with AgNW S/D nanoelectrodes proves that individual AgNWs can work as nanoelectrodes of large-scale electronic device arrays.

Not only 1D line-type AgNW nanoelectrode array, but also 2D sheet-type AgNW grids are effective alternative transparent electrodes for optoelectronic applications. Phosphorescent green OLED devices with stripe-patterned AgNWs and poly(3,4-ethylenedioxythiophene) doped with poly(4-styrenesulfonate) (PEDOT:PSS) composite transparent electrodes (100 µm pitch) achieved higher luminance than the device with conventional ITO anode at the same current density (**Figure 4**a and Figure S13a, Supporting Information). As a result, the device

Every NW was fabricated by PCAMP. b) Transfer characteristics of all-NW FETs compared with P3HT NW FET based on vacuum-deposited Au thin film (channel length = 100 µm, channel width = 3000 µm) (inset: comparison of field-effect mobilities between P3HT NW FET with Au film and AgNW S/D electrodes). c) Schematic illustration of thin film FETs with AgNW S/D nanoelectrodes. d) Transfer characteristics of IZO FETs with AgNWs (channel length = 200 µm, channel width = 3000 µm, inset: specific device structure and output characteristics). Transfer characteristics of pentacene FETs with e) the various channel length from 30 to 250 µm and pristine AgNW S/D electrodes and f) channel length of 50 µm and PFDT-treated AgNW S/D electrodes (channel width = 3000 µm, inset: specific device structures).

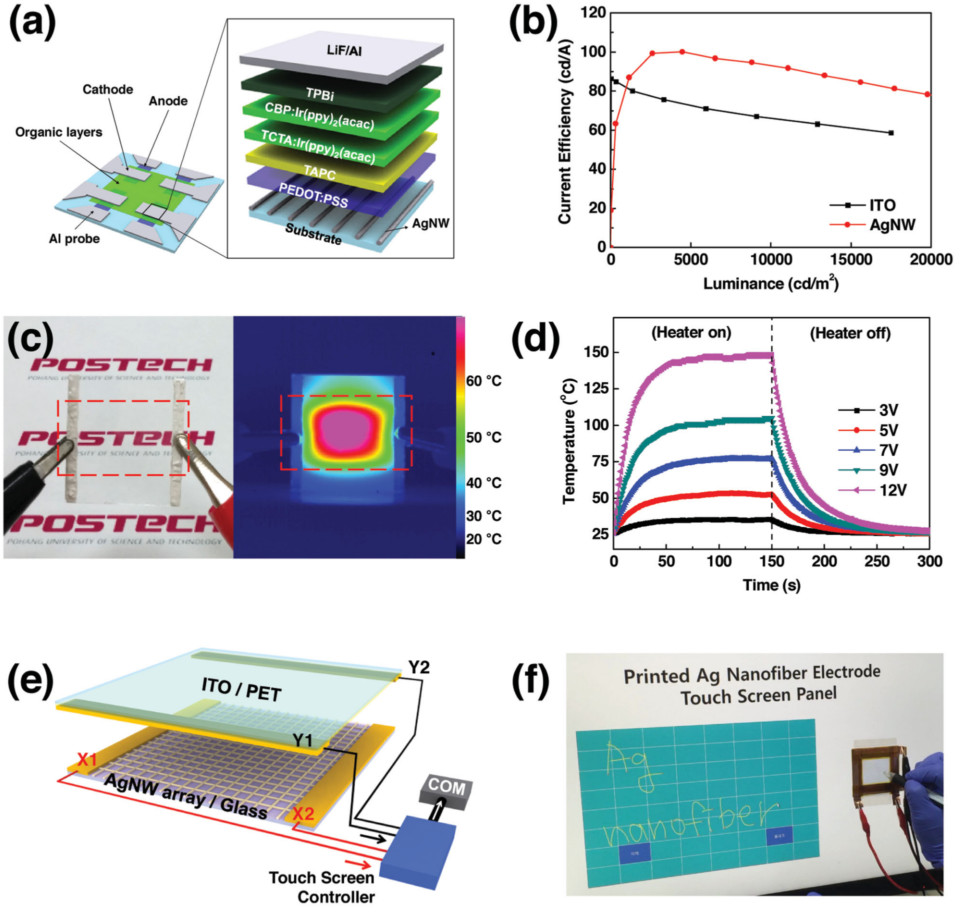

Figure 4. Electronic applications with AgNW array-based 2D transparent electrodes. a) Schematic illustration of OLED device with AgNW transparent electrode. b) Characteristics of current efficiency–luminance of ITO-based and AgNW-based OLED devices. c) Digital and IR images of AgNW-based transparent heater using stripe-patterned AgNW array with pitch size of 100 µm. The device showed uniform heat distribution. d) Temperature profile of AgNW-based transparent heater according to the applied voltage. e) Schematic illustration of TSP using grid-patterned AgNW array with pitch size of 300 µm. f) Demonstration of AgNW array-based TSP by writing words. The device worked well in repeated tests.

with the AgNW arrays showed higher maximum current efficiency (100.1 cd A^{-1}) than the ITO-based device (86.3 cd A^{-1}) (Figure 4b). The enhanced efficiency was because the reflective index of PEDOT:PSS on the AgNW array ($n_{\text{PEDOT:PSS}} \approx 1.5$) is lower than that of ITO ($n_{\text{ITO}} \approx 2.0$) and is well-matched with that of glass substrate ($n_{\text{Glass}} \approx 1.5$), so waveguided modes between anode and glass substrate can be effectively suppressed.[17,38] Moreover, nano-sized metallic wire structures with high density of free electrons can act as small light scattering spots to extract trapped photons from the device. To calculate the external quantum efficiencies (EQEs) of our devices, we measured the angular emission profiles (Figure S13b,c, Supporting Information). The maximum EQE of an AgNW-based OLED device was 25%, which was higher than that of the device with an ITO anode (maximum EQE = 20.7%).

Transparent heaters (Figure 4c,d) and TSPs (Figure 4e,f) with 2D sheet-type AgNW transparent electrodes were demonstrated based on high transparency and scalability of Ag nanowiring platform. Transparent NW heaters ($T \approx$ 97%) based on Joule heating effect were produced using stripe-patterned AgNWs array (100 µm pitch) printed on the middle part of a glass substrate (red dashed line box in Figure 4c,d). Silver paste was used to form a pair of contact electrodes to connect to a DC voltage generator (Figure 4c and Figure S14a, Supporting Information). The exothermic properties of the transparent heater were characterized using an infrared camera, which showed uniform heat distribution across the NW Joule heater while V_{IN} was applied (Figure 4c). We measured time-dependent temperature profile depending on input voltages 3 V ≤ V_{IN} ≤ 12 V (Figure 4d). The maximum temperature reached 77 °C at V_{IN} = 7 V, and 148 °C at V_{IN} = 12 V. The AgNWs heaters have a limited heating temperature up to 350 °C because AgNWs become gradually unstable above 350 °C and a considerable amount of heat is dissipated to the surrounding environment due to high surface to volume ratio and aspect ratio of NWs, unlike the bulk system of Joule heating.[39] So, it is difficult to estimate the ideal maximum heating temperature in our NW heater. However, the heating properties can be enhanced if the dissipated heat to surrounding decreases by revising the design of the NW heater, which includes the density and the pattern of NWs, the substrate and the passivation layer. Nonetheless, our highly transparent heater based on AgNWs can be a promising candidate for defrosters on automobile windshields, building windows, and bathroom mirrors.

A four-wire resistive type transparent TSP consisted of a bottom electrode of grid-patterned AgNW array with 300 µm pitch on a glass substrate, and a top electrode of ITO on a PET substrate (Figure 4e and Figure S14b, Supporting Information); a thin layer of PEDOT:PSS was coated on AgNW arrays as a protective conducting layer. Silver paste and copper tape were used to make effective contact terminals through which to apply a voltage to both electrodes. We tested TSP device by writing letters (Figure 4f) and the device worked very well repeatedly without noticeable degradation (Movie S1, Supporting Information). These results indicate that the printed AgNW (Type III) array for transparent electrodes has a potential of transparent and moiré-fringe-free optoelectronic applications.

In conclusion, we developed a novel Ag nanowiring platform for producing individually controllable, large-scale and long continuous AgNWs (Type III) which can overcome many limitations of conventional AgNWs (Types I and II). Utilizing AgNWs with an average diameter of 695 nm and low resistivity (5.7 µΩ cm) as 1D line-type nanoelectrodes, we successfully demonstrated various kinds of FETs, most notably the first all-NW FETs, by using direct printing method; all-NW FET showed a very high field-effect mobility of 2.08 cm^2 V^{-1} s^{-1}. By precise controlling the position and orientation of AgNWs during printing, we also produced 2D sheet-type AgNW transparent electrodes ($R_S \approx 26.9\ \Omega\ \square^{-1}$; haze ≈1% at $T \approx 94.7\%$) for OLEDs, transparent heaters, and TSPs. These results suggest that novel Ag nanowiring can provide a new promising and versatile platform for 1D nanoelectrodes of large-scale device arrays and for 2D sheet-type transparent electrodes of transparent optoelectronic devices. Furthermore, because the preparation of randomly coiled metal NWs using electrospinning has been widely studied, we expect that our individually controlled, highly aligned, and customizable metal nanowiring platform would not be limited only to Ag, but be extended to other metals such as ferromagnetic Fe, Co, and Ni.[6] Therefore, we also expect that this technology might immensely expand applications of printed nanoelectronics to electronic textiles and flexible optoelectronics in the near future.

Supporting Information

Supporting Information is available from the Wiley Online Library or from the author.

Acknowledgements

Y.L. and S.-Y.M. contributed equally to this work. This work was supported by the Center for Advanced Soft-Electronics funded by the Ministry of Science, ICT and Future Planning as Global Frontier Project (2014M3A6A5060947). This research was also supported by the MSIP (Ministry of Science, ICT and Future Planning), Korea, under the "ICT Consilience Creative Program" (IITP-R0346-16-1007) supervised by the IITP (Institute for Information & communications Technology Promotion). Y.L. thanks to Dr. Seawoong Lee in GIFT (Graduate Institute of Ferrous Technology) for kind help in measurement of transparent heaters.

Received: May 31, 2016
Revised: July 16, 2016

---

[1] a) M. Vosgueritchian, J. B.-H. Tok, Z. Bao, *Nat. Photonics* **2013**, *7*, 769; b) B. H. Hong, S. C. Bae, C.-W. Lee, S. Jeong, K. S. Kim, *Science* **2001**, *294*, 348; c) Y. Sun, B. Gates, B. Mayers, Y. Xia, *Nano Lett.* **2002**, *2*, 165; d) Y. Sun, B. Mayers, T. Herricks, Y. Xia, *Nano Lett.* **2003**, *3*, 955.

[2] a) J.-H. Chang, K.-M. Chiang, H.-W. Kang, W.-J. Chi, J.-H. Chang, C.-I. Wu, H.-W. Lin, *Nanoscale* **2015**, *7*, 4572; b) Y.-J. Shiau, K.-M. Chiang, H.-W. Lin, *Nanoscale* **2015**, *7*, 12698.

[3] W. Gaynor, S. Hofmann, M. G. Christoforo, C. Sachse, S. Mehra, A. Salleo, M. D. McGehee, M. C. Gather, B. Lüssem, L. Müller-Meskamp, P. Peumans, K. Leo, *Adv. Mater.* **2013**, *25*, 4006.

[4] Z. Yu, Q. Zhang, L. Li, Q. Chen, X. Niu, J. Liu, Q. Pei, *Adv. Mater.* **2011**, *23*, 664.

[5] a) H. Lee, S.-H. Choi, S. M. Jo, D. Y. Kim, S. Kwak, M. W. Cha, I.-D. Kim, S.-Y. Jang, *J. Phys. D: Appl. Phys.* **2009**, *42*, 125409; b) S.-H. Choi, T.-S. Hyun, H. Lee, S.-Y. Jang, S.-G. Oh, I.-D. Kim, *Electrochem. Solid-State Lett.* **2010**, *13*, A65.

[6] H. Wu, R. Zhang, X. Liu, D. Lin, W. Pan, *Chem. Mater.* **2007**, *19*, 3506.

[7] M. Bognitzki, M. Becker, M. Graeser, W. Massa, J. H. Wendorff, A. Schaper, D. Weber, A. Beyer, A. Gölzhäuser, A. Greiner, *Adv. Mater.* **2006**, *18*, 2384.

[8] M. Park, J. Im, M. Shin, Y. Min, J. J. Park, H. Cho, S. Park, M.-B. Shim, S. Jeon, D.-Y. Chung, J. Bae, J. J. Park, U. Jeong, K. Kim, *Nat. Nanotechnol.* **2012**, *7*, 803.

[9] a) H. Wu, D. Lin, R. Zhang, W. Pan, *Chem. Mater.* **2007**, *19*, 1895; b) W. Wang, Z. Feng, W. Jiang, J. Zhan, *CrystEngComm* **2013**, *15*, 1339.

[10] P.-C. Hsu, D. Kong, S. Wang, H. Wang, A. J. Welch, H. Wu, Y. Cui, *J. Am. Chem. Soc.* **2014**, *136*, 10593.

[11] a) S. Liu, J. B.-H. Tok, Z. Bao, *Nano Lett.* **2005**, *5*, 1071; b) M.-S. Lee, K. Lee, S.-Y. Kim, H. Lee, J. Park, K.-H. Choi, H.-K. Kim, D.-G. Kim, D.-Y. Lee, S. Nam, J.-U. Park, *Nano Lett.* **2013**, *13*, 2814.

[12] J.-Y. Lee, S. T. Connor, Y. Cui, P. Peumans, *Nano Lett.* **2008**, *8*, 689.

[13] a) J. H. Oh, H. W. Lee, S. Mannsfeld, R. M. Stoltenberg, E. Jung, Y. W. Jin, J. M. Kim, J.-B. Yoo, Z. Bao, *Proc. Natl. Acad. Sci. USA* **2009**, *106*, 6065; b) J. Y. Kim, B. H. Kim, J. O. Hwang, S.-J. Jeong, D. O. Shin, J. H. Mun, Y. J. Choi, H. M. Jin, S. O. Kim, *Adv. Mater.* **2013**, *25*, 1331; c) N. O. Weiss, X. Duan, *Nat. Nanotechnol.* **2013**, *8*, 312.

[14] S.-Y. Min, T.-S. Kim, B. J. Kim, H. Cho, Y.-Y. Noh, H. Yang, J. H. Cho, T.-W. Lee, *Nat. Commun.* **2013**, *4*, 1773.

[15] a) Y. Lee, T.-S. Kim, S.-Y. Min, W. Xu, S.-H. Jeong, H.-K. Seo, T.-W. Lee, *Adv. Mater.* **2014**, *26*, 8010; b) W. Xu, Y. Lee, S.-Y. Min, C. Park, T.-W. Lee, *Adv. Mater.* **2016**, *28*, 527; c) C. Song, J. A. Rogers, J.-M. Kim, H. Ahn, *Macromol. Res.* **2015**, *23*, 118; d) W. Xu, H.-K. Seo, S.-Y. Min, H. Cho, T.-S. Lim, C.-y. Oh, Y. Lee, T.-W. Lee, *Adv. Mater.* **2014**, *26*, 3459; e) S.-Y. Min, T.-S. Kim, Y. Lee, H. Cho, W. Xu, T.-W. Lee, *Small* **2015**, *11*, 45; f) H. Cho, S.-H. Jeong, S.-Y. Min, T.-H. Han, M.-H. Park, Y.-H. Kim, W. Xu, T.-W. Lee, *Adv. Optical Mater.* **2016**, *4*. 967.

[16] a) D. Kim, S. Jeong, H. Shin, Y. Xia, J. Moon, *Adv. Mater.* **2008**, *20*, 3084; b) D.-H. Youn, S.-H. Kim, Y.-S. Yang, S.-C. Lim, S.-J. Kim, S.-H. Ahn, H.-S. Sim, S.-M. Ryu, D.-W. Shin, J.-B. Yoo, *Appl. Phys. A* **2009**, *96*, 933; c) C. Kim, M. Nogi, K. Suganuma, *J. Micromech. Microeng.* **2012**, *22*, 035016; d) A. L. Dearden, P. J. Smith, D.-Y. Shin,

N. Reis, B. Derby, P. O'Brien, *Macromol. Rapid Commun.* **2005**, *26*, 315.

[17] L. Zhou, H. Xiang, S. Shen, Y. Li, J.-D. Chen, H. Xie, I. A. Goldthorpe, L. Chen, S. Lee, J. Tang, *ACS Nano* **2014**, *8*, 12796.

[18] H. Im, S. Jung, J. Jin, D. Lee, J. Lee, D. Lee, J. Lee, I.-D. Kim, B.-S. Bae, *ACS Nano* **2014**, *8*, 10973.

[19] S. Hong, J. Yeo, G. Kim, D. Kim, H. H. Lee, J. Kwon, H. H. Lee, P. Lee, S. H. Ko, *ACS Nano* **2013**, *7*, 5024.

[20] Y. Jang, J. Kim, D. Byun, *J. Phys. D: Appl. Phys.* **2013**, *46*, 155103.

[21] H.-Z. Geng, K. K. Kim, K. P. So, Y. S. Lee, Y. Chang, Y. H. Lee, *J. Am. Chem. Soc.* **2007**, *129*, 7758.

[22] T.-H. Han, Y. Lee, M.-R. Choi, S.-H. Woo, S.-H. Bae, B. H. Hong, J.-H. Ahn, T.-W. Lee, *Nat. Photonics* **2012**, *6*, 105.

[23] H. Kim, S.-H. Bae, T.-H. Han, K.-G. Lim, J.-H. Ahn, T.-W. Lee, *Nanotechnology* **2014**, *25*, 014012.

[24] a) W. M. Wang, R. M. Stoltenberg, S. Liu, Z. Bao, *ACS Nano* **2008**, *2*, 2135; b) Y.-C. Chang, H.-C. Chung, S.-C. Lu, T.-F. Guo, *Nanotechnology* **2013**, *24*, 095302; c) J. Sung, P. S. Jo, H. Shin, J. Huh, B. G. Min, D. H. Kim, C. Park, *Adv. Mater.* **2008**, *20*, 1505.

[25] a) J.-U. Park, M. Hardy, S. J. Kang, K. Barton, K. Adair, D. K. Mukhopadhyay, C. Y. Lee, M. S. Strano, A. G. Alleyne, J. G. Georgiadis, P. M. Ferreira, J. A. Rogers, *Nat. Mater.* **2007**, *6*, 782; b) M. S. Onses, C. Song, L. Williamson, E. Sutanto, P. M. Ferreira, A. G. Alleyne, P. F. Nealey, H. Ahn, J. A. Rogers, *Nat. Nanotechnol.* **2013**, *8*, 667.

[26] S. Jung, S. Lee, M. Song, D.-G. Kim, D. S. You, J.-K. Kim, C. S. Kim, T.-M. Kim, K.-H. Kim, J.-J. Kim, J.-W. Kang, *Adv. Energy Mater.* **2014**, *4*, 1300474.

[27] K. S. Kim, Y. Zhao, H. Jang, S. Y. Lee, J. M. Kim, K. S. Kim, J.-H. Ahn, P. Kim, J.-Y. Choi, B. H. Hong, *Nature* **2009**, *457*, 706.

[28] D. Tobjörk, N. J. Kaihovirta, T. Mäkelä, F. S. Pettersson, R. Österbacka, *Org. Electron.* **2008**, *9*, 931.

[29] S. Rentenberger, A. Vollmer, E. Zojer, R. Schennach, N. Koch, *J. Appl. Phys.* **2006**, *100*, 053701.

[30] M.-R. Choi, T.-H. Han, K.-G. Lim, S.-H. Woo, D. H. Huh, T.-W. Lee, *Angew. Chem.* **2011**, *123*, 6398.

[31] B. de Boer, A. Hadipour, M. M. Mandoc, T. van Woudenbergh, P. W. M. Blom, *Adv. Mater.* **2005**, *17*, 621.

[32] F. P. Koffyberg, F. A. Benko, *J. Appl. Phys.* **1982**, *53*, 1173.

[33] H.-W. Chang, Y.-C. Tsai, C.-W. Cheng, C.-Y. Lin, Y.-W. Lin, T.-M. Wu, *J. Colloid Interface Sci.* **2011**, *360*, 305.

[34] D. P. Dubal, G. S. Gund, R. Holze, H. S. Jadhav, C. D. Lokhande, C.-J. Park, *Dalton Trans.* **2013**, *42*, 6459.

[35] D. V. Demidov, I. P. Prosvirin, A. M. Sorokin, V. I. Bukhtiyarov, *Catal. Sci. Technol.* **2011**, *1*, 1432.

[36] J.-Y. Kwon, D.-J. Lee, K.-B. Kim, *Electron. Mater. Lett.* **2011**, *7*, 1.

[37] Y. Gao, J. Lu, J. Zhang, X. Li, *RSC Adv.* **2015**, *5*, 37635.

[38] M. Cai, Z. Ye, T. Xiao, R. Liu, Y. Chen, R. W. Mayer, R. Biswas, K.-M. Ho, R. Shinar, J. Shinar, *Adv. Mater.* **2012**, *24*, 4337.

[39] a) C. Y. Jin, Z. Li, R. S. Williams, K.-C. Lee, I. Park, *Nano Lett.* **2011**, *11*, 4818; b) F. Léonard, *Appl. Phys. Lett.* **2011**, *98*, 103101.